Ordered Liquid Aluminum at the Interface with Sapphire

S. H. Oh,[1*] Y. Kauffmann,[2*] C. Scheu,[1,3] W. D. Kaplan,[2†] M. Rühle[1]

Understanding the nature of solid-liquid interfaces is important for many processes of technological interest, such as solidification, liquid-phase epitaxial growth, wetting, liquid-phase joining, crystal growth, and lubrication. Recent studies have reported on indirect evidence of density fluctuations at solid-liquid interfaces on the basis of x-ray scattering methods that have been complemented by atomistic simulations. We provide evidence for ordering of liquid atoms adjacent to an interface with a crystal, based on real-time high-temperature observations of alumina-aluminum solid-liquid interfaces at the atomic-length scale. In addition, crystal growth of alumina into liquid aluminum, facilitated by interfacial transport of oxygen from the microscope column, was observed in situ with the use of high-resolution transmission electron microscopy.

Evidence of density fluctuations at solid-liquid interfaces based on x-ray scattering methods (*1*–*5*) and atomistic simulations (*6*–*11*) has promoted interest in fundamental studies of the structure of solid-liquid interfaces. A limited number of studies have been conducted by high-resolution transmission electron microscopy (HRTEM) (*12*–*16*) because of the need for suitable microscopes and material systems that facilitate the study of such experimentally challenging systems. In principle, a liquid metal in contact with a solid ceramic substrate could serve as a model system for in situ HRTEM of solid-liquid interfaces. Earlier work on electron irradiation damage of ceramics has shown that damage processes occurring in alumina (Al_2O_3) during transmission electron microscopy (TEM) studies induce the appearance of metallic aluminum (Al) in the form of interstitial dislocation loops, precipitates, or crystallites, as a result of electronic transition and/or ballistic knock-on displacement mechanisms (*17*, *18*). During irradiation with a high-voltage electron microscope (HVEM), the different threshold displacement energies of Al and oxygen mainly account for the selective displacement of Al ions (*19*, *20*). In situ heating in HVEM further accelerates the irradiation damage of alumina, resulting in the formation of liquid Al drops (*21*).

In this study, in situ heating TEM experiments were performed in the Max-Planck-Institut–Stuttgart high-voltage atomic resolution TEM (JEM-ARM 1250, Japanese Electron Optics Laboratory, Inc.) operating at 1.25 MeV. This 0.12-nm-point resolution microscope (*22*) is equipped with a hot-stage and a drift compensator, enabling highly stable working conditions at elevated temperatures up to 1000°C, and an electron energy loss spectroscopy (EELS) detector [Gatan Image Filter (*23*)] for analytical characterization. All experimental work done for this study was conducted between 660° and 800°C (the melting point of Al is ~660°C) and recorded on negatives or on a real-time (25 frames per second) charge-coupled device video camera. Experimental observations were obtained from pure single crystalline alumina (α-Al_2O_3, sapphire) specimens with different crystalline orientations, prepared by conventional dimpling and Ar ion thinning methods (*24*).

During the examination of the specimens by HVEM and at two temperatures above the melting point of Al, two parallel processes were observed. In some regions, dissociation of the alumina was observed, and in other areas liquid aluminum droplets formed on the alumina specimen (Fig. 1A).

The dissociation of the alumina is probably due to knock-on displacement damage processes that cause oxygen atoms to be knocked out of the alumina into the microscope column, leaving the aluminum atoms behind (*19*, *20*). Above the melting point of Al, the unoxidized Al atoms rapidly diffuse to the free surface and form liquid Al droplets on the alumina specimen.

The liquid drops at the edge of the Al_2O_3 crystal can form different interface morphologies, such as those presented schematically in Fig. 1B. All of these interface morphologies were observed. However, only the configuration schematically shown in panel 1 of Fig. 1B provides an interface that can be interpreted by HRTEM, and only data from such interface morphologies are presented here. This was carefully checked during the experiments and subsequently confirmed by HRTEM image simulations.

Electron diffraction patterns of the droplets showed the existence of diffuse scattering rings, typical for short-range order in a liquid phase. Careful analysis of the chemical composition of the liquid droplets in situ, with the use of EELS at 800°C (fig. S1), and ex situ analysis of the solid droplets with a dedicated scanning transmission electron microscope (STEM) (VG HB-501-UX) equipped with an EELS [UHV Enfina (*23*)], confirmed that these droplets are in fact pure aluminum, and no oxygen or other elements were detected within the detection limits (~1.0 atomic %). The chemical state was further probed ex situ by EELS plasmon mapping (fig. S2). The plasmon peaks of Al and α-Al_2O_3 appear at 15 and 26 eV, respectively, and provide information on the oxidation state of Al. The metallic Al state was detected in the droplets, and only a thin native oxide skin was detected at the surface of the droplets.

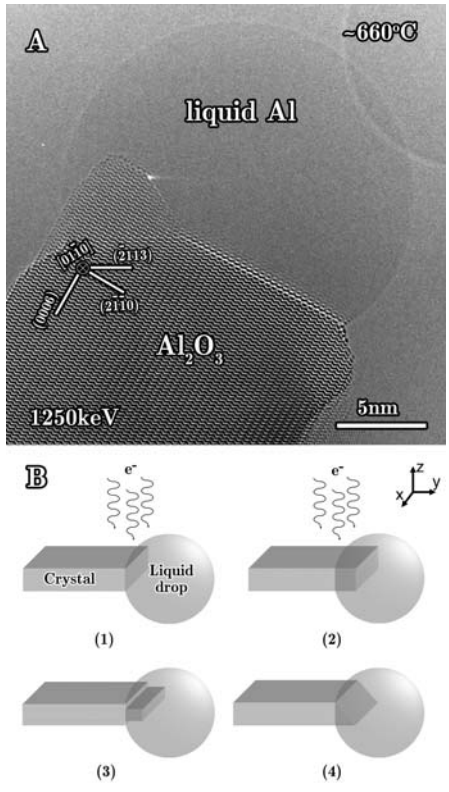

Fig. 1. Formation of an aluminum liquid droplet on an alumina TEM specimen. (**A**) Experimental HRTEM image of an aluminum liquid droplet formed on an alumina TEM specimen at ~660°C. The thickness of the crystal is estimated to be ~20 nm (which is approximately the diameter of the droplet). (**B**) Schematic representation of some of the possible interface morphologies formed at the liquid-crystal contact area: (1) Flat edge-on interface. The drop is attached to the substrate at the edge of the crystal, on the facet parallel to the *z* axis. (2) Buried interface inside the liquid. The drop covers the crystal from all directions so the interface of interest is buried inside the drop. (3) Ledge formation. Because of surface roughness and/or different rates of crystal growth, ledges are formed at the interface. (4) An inclined interface.

[1]Max-Planck-Institut für Metallforschung, 70569 Stuttgart, Germany. [2]Department of Materials Engineering, Technion–Israel Institute of Technology, Haifa 32000, Israel. [3]Now Department of Physical Metallurgy and Materials Testing, University of Leoben, A-8700 Leoben, Austria.

*These authors contributed equally to this work.
†To whom correspondence should be addressed. E-mail: kaplan@tx.technion.ac.il

The occurrence of these pure liquid aluminum droplets on the crystalline alumina provides a unique opportunity to probe wetting dynamics at the atomistic level and makes this system suitable for the study of interesting structural phenomena occurring at solid-liquid interfaces. We addressed an intriguing question: What is happening immediately at the interface between the crystal and the liquid at the atomic level? Real-time movies recorded during the in situ heating experiments show a dynamical evolution of the interface. Image analysis of two successive movie images demonstrates layer-by-layer crystal growth into the liquid through ledge migration (Fig. 2). The velocity of the ledge is estimated to be not less than 4×10^{-5} cm/s at 750°C (within the time resolution of the video system, 0.04 s).

In addition, along the solid-liquid interface, periodic contrast perturbations are evident (Fig. 3) both perpendicular and parallel to the interface. These contrast perturbations were observed repeatedly (in different specimens and different crystallographic orientations) and under different imaging conditions (objective lens defocus), showing the reproducibility of such observations. The most important question is whether these contrast perturbations are due to ordering in the liquid or caused by imaging artifacts such as delocalization, objective lens defocus, and/or interface inclination.

Delocalization is an imaging artifact that can be notable in high-resolution images, which means that image details are displaced from their true locations in the specimen (*25*). For example, if we look at a line scan across a simulated HRTEM image of an alumina-vacuum interface calculated with the multislice method (*26*) and for the same imaging conditions as the experimental data (the black line in Fig. 4), we observe contrast perturbations in the vacuum which are caused by the delocalization effect. However, inspection of the periodicity of the delocalization fringes and the ones observed in the experimental micrographs (red dots in Fig. 4 and fig. S3, A and B) shows that the periodicities are totally different. To rule out the possibility that this contrast could be generated by delocalization when a "perfect" (completely disordered)

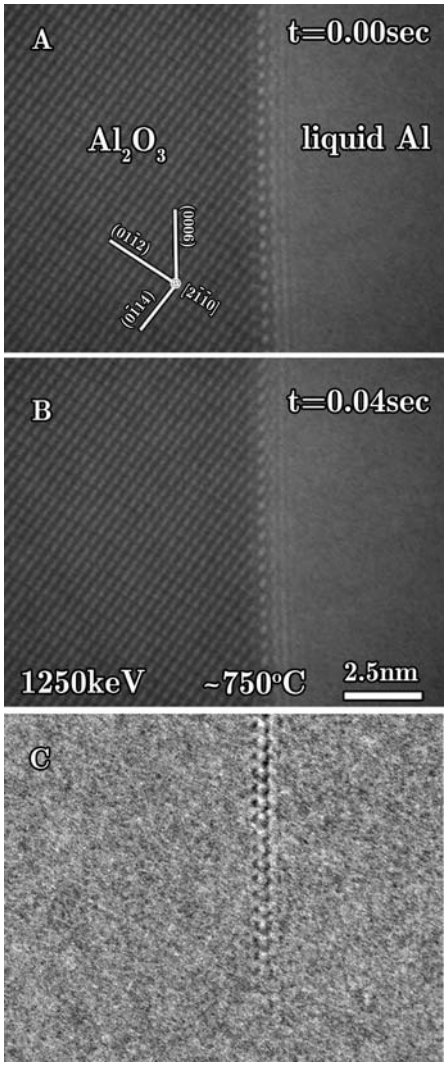

Fig. 2. Frame-by-frame HRTEM images of the solid-liquid interface illustrating the ledge migration motion. The frame images (**A**) and (**B**) were captured from the real-time movie (movie S1) recorded at ~750°C in a time sequence of 0.04 s. Any specimen drift contribution to the motion of the image was completely canceled out by the drift compensator device attached to the microscope. (**C**) Difference image obtained by subtracting image (A) from image (B).

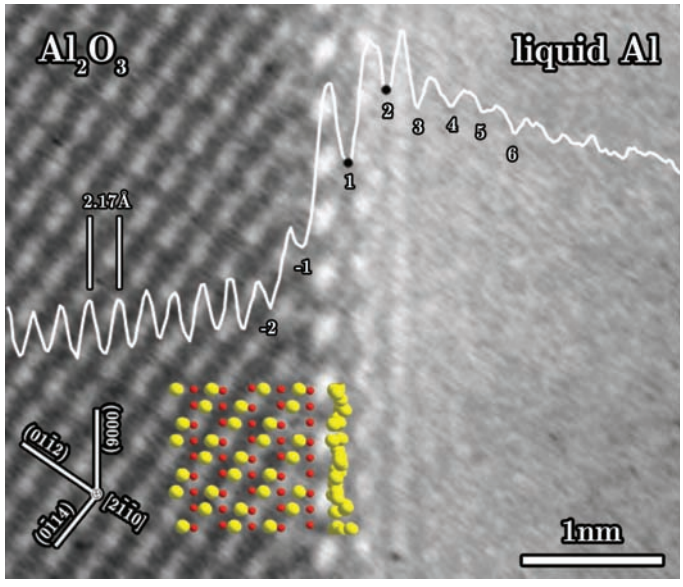

Fig. 3. Magnified area from a movie image acquired at ~750°C showing the contrast perturbations in the liquid parallel to the (0006) planes in alumina. The atom positions in the Al_2O_3 (red for oxygen and yellow for aluminum) were determined by contrast matching between simulated and experimental images at different objective lens defocus and specimen thickness values. The first layer of liquid atoms is shown schematically. The white line is an average-intensity line scan perpendicular to the interface. The numbers indicate the minima in intensity, which for the negative numbers correlate to the columns of atoms in the sapphire and for the positive numbers correlate to the intensity perturbations in the Al. The two black points at 1 and 2 indicate identified layers of ordered liquid Al.

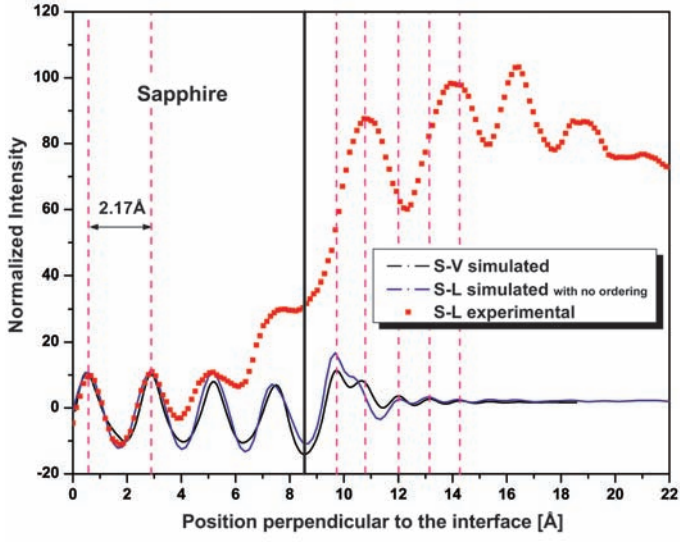

Fig. 4. Comparisons between the (normalized) intensity line scans from the solid-liquid experimental image (red squares), a solid-vacuum simulated image (black curve), and an artificial solid-liquid simulated interface which contains no ordering at all (blue curve) (fig. S3, C and D). All images were simulated with imaging parameters matching the experimental conditions (including thermal vibrations due to the high temperature), which were determined by iteratively matching simulated images with the experimental image of alumina (away from the interface). The vertical black line indicates the position of the interface between the crystal and the vapor/liquid.

liquid is present, a HRTEM micrograph of the interface was simulated using atomic coordinates of a perfect alumina crystal adjacent to liquid aluminum generated from molecular dynamics simulations (*27*) at a temperature of 927°C. The line scan across this interface is represented by the blue line in Fig. 4 (see also fig. S3, C and D) and shows a similar periodicity to that of the solid-vacuum interface. These comparisons show that the contrast perturbations observed in the experimental micrographs are not due only to delocalization but rather a convolution of this effect (which is always present) with ordering in the liquid. Another reasonable possibility is that these contrast perturbations are due to interface inclination or ledge growth (as shown schematically in panels 3 and 4 of Fig. 1B). However, detailed image simulations showed that for inclined interfaces or interfaces containing ledges, a gradual decrease in contrast near the interface would be seen, with a contrast very different from that generated by an interface between a crystal and a partially ordered liquid.

Measurements of the spacing between the last layer of the crystal (marked as –1) and the first contrast perturbation in the liquid (marked as 1), from the image shown in Fig. 3, result in a distance (±SD) of ~3.5 ± 0.25 Å. The next spacing between the contrast perturbations (marked as 1 and 2) is 2.85 ± 0.25 Å. Subsequent spacings in the liquid further decrease until they reach the spacing of (0006) planes in alumina (~2.17 Å), within the error range of the measurement (determined by the pixel size). The large change in spacing right at the interface may be caused by delocalization and/or the formation of a transient phase caused by oxygen transport along the interface (*28*, *29*). This can be determined only by deconvoluting the influence of delocalization from the image contrast.

The results presented here provide evidence that crystals can induce ordering in liquids, even in high-temperature metal-ceramic systems. For the specific system in case, oxygen from the microscope column permeates the ordered liquid along the interface, and then is deposited as Al_2O_3 by epitaxial growth, facilitated by the motion of interfacial steps. This indicates that crystal-induced ordering of liquids may play an important role in liquid phase epitaxial growth, as well as high temperature wetting. Although ordering in the form of layers of Al atoms parallel to the interface with the crystal was clearly detected, the time-averaged positions of the liquid atoms require further advanced TEM imaging techniques and comparison with computer simulations. Of particular interest is the degree of in-plane order (*11*) and comparison of the local atomistic structure in the liquid with the solidified interface and with Al-Al_2O_3 interfaces formed by other processing methods (*30*).

References and Notes

1. O. M. Magnussen *et al.*, *Phys. Rev. Lett.* **74**, 4444 (1995).
2. H. Reichert *et al.*, *Nature* **408**, 839 (2000).
3. W. J. Huisman *et al.*, *Nature* **390**, 379 (1997).
4. C. J. Yu, A. G. Richter, A. Datta, M. K. Durbin, P. Dutta, *Phys. Rev. Lett.* **82**, 2326 (1999).
5. A. K. Doerr, M. Tolan, J. P. Schlomka, W. Press, *Europhys. Lett.* **52**, 330 (2000).
6. T. P. Swiler, R. E. Loehman, *Acta Materialia* **48**, 4419 (2000).
7. F. F. Abraham, Y. Singh, *J. Chem. Phys.* **67**, 2384 (1977).
8. J. Q. Broughton, G. H. Gilmer, *J. Chem. Phys.* **84**, 5749 (1986).
9. E. T. Chen, R. N. Barnett, U. Landman, *Phys. Rev. B* **40**, 924 (1989).
10. R. L. Davidchack, B. B. Laird, *Phys. Rev. Lett.* **85**, 4751 (2000).
11. A. Hashibon, J. Adler, M. W. Finnis, W. D. Kaplan, *Interface Sci.* **9**, 175 (2001).
12. J. M. Howe, H. Saka, *MRS Bull.* **29**, 951 (2004).
13. J. M. Howe, *Philos. Mag. A* **74**, 761 (1996).
14. S. E. Donnelly *et al.*, *Science* **296**, 507 (2002).
15. S. Arai, S. Tsukimoto, S. Muto, H. Saka, *Microsc. Microanal.* **6**, 358 (2000).
16. H. Saka, K. Sasaki, S. Tsukimoto, S. Arai, *J. Mater. Res.* **20**, 1629 (2005).
17. J. E. Bonevich, L. D. Marks, *Ultramicroscopy* **35**, 161 (1991).
18. G. Dehm, K. Nadarzinski, F. Ernst, M. Rühle, *Ultramicroscopy* **63**, 49 (1996).
19. G. P. Pells, D. C. Phillips, *J. Nucl. Mater.* **80**, 207 (1979).
20. G. P. Pells, D. C. Phillips, *J. Nucl. Mater.* **80**, 215 (1979).
21. G. P. Pells, *Journal of the American Ceramic Society* **77**, 368 (1994).
22. F. Phillipp, R. Höschen, M. Osaki, G. Möbus, M. Rühle, *Ultramicroscopy* **56**, 1 (1994).
23. Gatan, Inc., Pleasanton, CA.
24. A. Strecker *et al.*, *Zeitschrift Für Metallkunde* **94**, 290 (2003).
25. M. T. Otten, W. M. J. Coene, *Ultramicroscopy* **48**, 77 (1993).
26. P. A. Stadelmann, *Ultramicroscopy* **21**, 131 (1987).
27. F. Ercolessi, J. B. Adams, *Europhys. Lett.* **26**, 583 (1994).
28. G. Levi, W. D. Kaplan, *Acta Materialia* **50**, 75 (2002).
29. M. Hoch, H. L. Johnston, *J. Am. Chem. Soc.* **76**, 2560 (1954).
30. G. Dehm, B. J. Inkson, T. Wagner, *Acta Materialia* **50**, 5021 (2002).

31. We thank F. Phillipp and J. M. Howe for discussions and U. Salzberger, R. Höschen, and J. Thomas for technical assistance. This work was partially funded by the German-Israel Fund (grant I-779-42.10/2003), the German Science Foundation through the Graduiertenkolleg Innere Grenzflächen (GRK 285/3), and the Russell Berrie Nanotechnology Institute at the Technion.

Supporting Online Material

www.sciencemag.org/cgi/content/full/1118611/DC1
Materials and Methods
Figs. S1 to S3
References
Movie S1

9 August 2005; accepted 21 September 2005
Published online 6 October 2005;
10.1126/science.1118611
Include this information when citing this paper.

Stem-Cell Homeostasis and Growth Dynamics Can Be Uncoupled in the *Arabidopsis* Shoot Apex

G. Venugopala Reddy and Elliot M. Meyerowitz*

The shoot apical meristem (SAM) is a collection of stem cells that resides at the tip of each shoot and provides the cells of the shoot. It is divided into functional regions. The central zone (CZ) at the tip of the meristem is the domain of expression of the *CLAVATA3* (*CLV3*) gene, encoding a putative ligand for a transmembrane receptor kinase, CLAVATA1, active in cells of the rib meristem (RM), located just below the CZ. We show here that CLV3 restricts its own domain of expression (the CZ) by preventing differentiation of peripheral zone cells (PZ), which surround the CZ, into CZ cells and restricts overall SAM size by a separate, long-range effect on cell division rate.

Pattern formation in the SAM is a dynamic process that results from active orchestration of spatial and temporal patterns of gene expression and of cellular behavior, by cell-cell communication. In *Arabidopsis thaliana*, the SAM consists of several hundred cells divided into functional domains that are characterized by different cellular behaviors and by different patterns of gene expression (*1*, *2*). Progeny of CZ cells enter into differentiation pathways when they enter the surrounding meristematic regions: the flanking PZ, where leaf and flower primordia are formed, and the RM beneath the CZ, where cells of the stem form. The functional domains of the SAM, CZ, PZ, and RM are established in embryonic development and maintain their relative proportions throughout postembryonic life, even though cells are continually diverted to differentiation pathways. The cells of the CZ signal to the RM by producing the product of the *CLV3* gene, a small extracellular protein thought to be the ligand for the CLAVATA1 receptor kinase, expressed in some RM cells (*3*, *4*). CLV1 acts, at least in part, by down-regulating the activity of the homeodomain protein WUSCHEL (WUS), also expressed in some RM cells (*5*, *6*). WUS acts, in turn, to up-regulate *CLV3* expression in the overlying CZ by means of an unknown diffusible signal (*7*). CLV3 thus

California Institute of Technology, Division of Biology, MC 156-29, 1200 East California Boulevard, Pasadena, CA 91125, USA.

*To whom correspondence should be addressed. E-mail: meyerow@its.caltech.edu